Metal/metalloid and phosphorus characteristics in porewater associated with manganese geochemistry: A case study in the Jiulong River Estuary, China[☆]

Feng Pan [a], Huatai Liu [b, *], Zhanrong Guo [a], Yu Cai [a], Yuyao Fu [a], Jinye Wu [a], Bo Wang [a], Aiguo Gao [a, c]

[a] College of Ocean and Earth Sciences, Xiamen University, Xiamen 361102, PR China
[b] College of the Environment and Ecology, Xiamen University, Xiamen 361102, PR China
[c] State Key Laboratory of Marine Environmental Science, Xiamen University, Xiamen 361102, PR China

A B S T R A C T

Sediment porewater can be an important source of contaminants in the overlying water, but the mechanisms of metal(loid) and phosphorus (P) remobilization remain to be investigated. In this study, high-resolution dialysis (HR-Peeper) and diffusive gradients in thin films (DGT) samplers were used to determine the porewater dissolved iron (Fe), manganese (Mn), cobalt (Co), chromium (Cr), vanadium (V), selenium (Se), arsenic (As), P and DGT-Labile S in coastal sediments in the Jiulong River Estuary (JRE), China. The results showed that high concentrations of dissolved Mn, Se and P were present in the overlying water, indicating potential water pollution with excessive amounts of Mn, Se and P. The dissolved Mn concentrations in the porewater were higher than the dissolved Fe concentrations, especially at submerged sites, demonstrating that Mn(III/IV) reduction is the dominant diagenetic pathway for organic carbon (OC) degradation, which directly affects Fe cycling by the competitive inhibition of Fe(III) reduction and Fe(II) reoxidation. Dissolved Co, Cr, V, Se, As and P show significant positive correlations with Mn but nearly no correlations with Fe, suggesting that the mobility of these metal(loid)s and P is associated with Mn but not Fe cycling in this region. In addition, the coelevated concentrations of the metal(loid)s, P and Mn at the submerged sites are attributed to the strengthened Mn reduction coupled with OC degradation fueled by hypoxia. The higher positive diffusion fluxes of Mn, Se and P were consistent with the excess Mn, Se and P concentrations in the overlying water, together with the approximately positive fluxes of the other metal(loid)s, indicating that sediment Mn(III/IV) reduction and concomitant metal(loid) and P remobilization might be vital pathways for metal(loid) and P migration to the overlying water.

© 2019 Elsevier Ltd. All rights reserved.

1. Introduction

The availability of bioessential trace elements such as iron (Fe), manganese (Mn), sulfur (S), cobalt (Co), chromium (Cr), vanadium (V) and selenium (Se) underpins the emergence, long-term evolution, and activity of life on our planet (Swanner et al., 2014), but excessive amounts of these elements can have negative and toxic effects on aquatic ecosystems because of their persistence and abiotic degradation in the environment and bioaccumulation in

food webs (Hamilton, 2004; Wang and Wang, 2017). Arsenic (As) is known as one of the most dangerous environmental hazards due to its adverse impact on human health and wide distribution in the environment (Sharma and Sohn, 2009; Sun et al., 2017). As one of the macronutrients required for life, an excess phosphorus (P) input also causes harmful environmental problems, such as eutrophication (Conley et al., 2009; Ding et al., 2018a). With the development of industrialization and urbanization, large amounts of metal(loid) and nutrient contaminants from industrial, urban, and agricultural sources have been transported into the ocean (Khademi et al., 2018; Wang and Wang, 2016). As the transitional region of land and ocean, estuarine and coastal areas are suffering from massive contamination, most of which are ultimately deposited along with

coastal sediments (Liu et al., 2019).

Sediments can act as both sources and sinks of contaminants to the overlying water columns, depending on the redox conditions and prevailing diagenetic processes in the sediments and porewater (Pan et al., 2019). Exogenetic metal(loid)s and P are usually present as adsorbed, coprecipitated and mineral phases formed through combination with various oxides and clay minerals in the sediments (Jia et al., 2007; Kraal et al., 2015). However, the contaminant characteristics of porewater reflect the geochemical cycling of the elements in sediments, and porewater is also a vital medium connecting the sediments and the overlying water (Ni et al., 2017). Diagenetic reactions that increase the dissolved contaminant concentrations by converting the solid phase to the porewater phase can therefore promote their liberation to the overlying water. In coastal sediments, these reactions are coupled to the oxidation of organic carbon (OC), especially when Fe/Mn (oxyhydr)oxides and S are the terminal electron acceptors (Kalnejais et al., 2015).

The geochemical cycles of the metal(loid)s and P in sediments and porewater are mainly controlled by Fe and Mn redox cycling (Sharma and Sohn, 2009; Rozan et al., 2002). Under oxic conditions, metal(loid)s and P are scavenged from the aqueous phase by Fe and Mn (hydr)oxides (Sundby, 2006). Under anoxic conditions, metal(loid)s and P can be remobilized and released into porewater from the reductive dissolution of iron/manganese oxides and/or reduction of the adsorbed and/or coprecipitated high-valent metal(loid)s to low-valent metal(loid)s (e.g., As(V) to As(III), Co(III) to Co(II), Cr(VI) to Cr(III)) (Bose and Sharma, 2002; Ellis et al., 2002; Leermakers et al., 2005; Swanner et al., 2014). In addition, sulfide formed by sulfate reduction can precipitate with heavy metals, thereby removing them from the porewater and immobilizing them (Muyzer and Stams, 2008). Fe (hydr)oxides are generally believed to be the dominant factor controlling metal(loid) and P mobility levels due to their ubiquitous presence in the supergene environment (Shaw et al., 1990; Bose and Sharma, 2002; Rozan et al., 2002). In recent studies, Mn oxides have been found to supersede Fe(III) oxides in trapping metal(loid)s such as As, Co, Zn and Cr, and their mobility is mainly controlled by the absorption and reductive dissolution of Mn oxides (Zhang et al., 2002; Beck et al., 2010; Jin et al., 2019; Fan et al., 2019). Mn plays a particularly significant role, presumably due to the greater sorptive capacity of its solid oxide surfaces for transition metal cations (Beck et al., 2010). Nevertheless, the study on Mn geochemistry-controlled metal(loid) mobility is scant and lacks visualized proof, especially in the marine sedimentary environment.

For redox-sensitive elements, *ex situ* porewater sampling methods, such as centrifugation and squeezing, might be unreliable due to artificial perturbations and sample oxidation (Kankanmge et al., 2017). In addition, the centimeter-scale resolution was considered inadequate for studying porewater processes because all steep concentration gradients will be averaged (Stockdale et al., 2009). Equilibrium dialysis sampling (Peeper) is an *in situ* sampling technique based on the principle of diffusion equilibrium (Teasdale et al., 1995). In recent years, improved high-resolution dialysis (HR-Peeper) has been widely used for porewater solute sampling to study the metal(loid)s and nutrients in freshwater systems (Xu et al., 2012; Chen et al., 2019a; Fan et al., 2019). However, works on metal(loid)s and nutrients using HR-Peeper are rare in coastal marine systems, which greatly restricts our further understanding of porewater geochemistry. The aim of this study was therefore to combine conventional sediment core analysis and the diffusive gradients in thin films (DGT) technique with a novel HR-Peeper instrument to reveal the metal(loid) and P behaviors in porewater and the sensitive fractions in sediments and their relationships with Mn, Fe and S redox geochemistry. The results obtained from

high-resolution sampling are beneficial for a better understanding of the geochemical cycling of metal(loid)s and P in coastal marine systems and their benthic exchange fluxes across the sediment-water interface (SWI).

2. Materials and methods

2.1. Description of the sampling sites

The Jiulong River Estuary (JRE) is a semienclosed bay located in Fujian Province, southern China. This estuary is a typical subtropical macrotidal system (Yang et al., 2012) with a mean tidal range of 4.1 m and a maximum tidal range of over 6 m. The mixed estuarine water is characterized by a high suspended particulate matter (particulate organic carbon (POC) content of more than $100\,\mu M$) together with a low concentration of dissolved oxygen (less than $7\,mg\,L^{-1}$) (Lin et al., 2013; Wu et al., 2017). Previous studies have found severe metal pollution in both the sediment porewater and overlying water due to industrial effluents (Wang and Wang, 2016; Wang and Wang, 2017). P pollution was also serious and was partly attributed to the release of sediment-hosted P (Pan et al., 2017; Pan et al., 2019).

Considering potential differences in redox conditions, organic matter distributions and bioturbation, six sites in the intertidal zone of a tidal creek were selected for the study (Fig. 1). Site 1 (JRE-1) was located in the mangrove forest where the location was flooded by the highest tide, site 2 (JRE-2) was located at the edge of
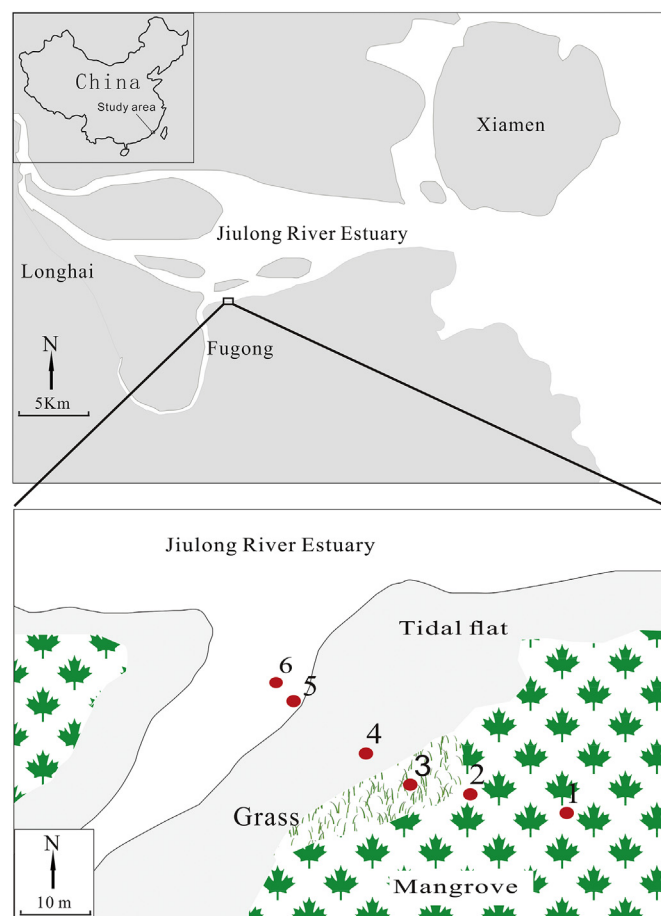

Fig. 1. Locations of the sampling sites during low-tide time in the coastal zones of the Jiulong River Estuary, China.

the mangrove forest, site 3 (JRE-3) was located in the grassland adjacent to the mangrove forest, site 4 (JRE-4) was located in the bare mudflat, site 5 (JRE-5) was located in the submerged area just below the lowest tide, and site 6 (JRE-6) was also located in the submerged area below JRE-5.

2.2. Preparation of HR-Peeper and sampling

The principle of Peeper involves the use of a dialysis membrane to separate multichambered receiver solutions from the surrounding porewater. Dissolved chemicals diffuse across the membrane and achieve equilibrium after some time; hence, the compositions of the receiver solutions are the same as those of the porewater (Teasdale et al., 1995). The improved HR-Peeper device used here contained 36 equally spaced $400\,\mu L$ chambers fully loaded with deionized water with a 5.0 mm vertical resolution, and the chamber surfaces were covered using cellulose nitrate membranes (Whatman, $0.45\,\mu m$ pore size) (Xu et al., 2012). The DGT technique is an *in situ* high-resolution technique for dynamically measuring labile species in sediments (Davison and Zhang, 1994), namely, dissolved sulfide (S^{2-}) for S. The HR-Peeper and ZrO-AgI DGT probes were provided by Easy Sensor Ltd. (www.easysensor. net). Prior to field deployment, all HR-Peeper and ZrO-AgI DGT devices were soaked and deoxygenated with nitrogen in deionized water and stored in the dark for at least 16 h.

During the low-tide period, the HR-Peeper probes were inserted into the sediment at six sampling sites (Fig. 1). The next day, the ZrO-AgI DGT devices were inserted into the same cores carefully. After being deployed for another full day, the HR-Peeper and ZrO-AgI DGT probes were removed from the sediment, and the surfaces of the probes were rinsed with deionized water. Subsequently, the solution in each chamber was retrieved, a portion of which was acidified with HNO_3 for metal(loid) determination. After retrieval of the HR-Peeper probes, sediment cores were collected using hollow PVC tubes. Then, each sediment core was sectioned at 1 cm (0−5 cm) or 2 cm intervals (5−15 cm). The samples were stored in nitrogen-filled polyethylene bags prior to laboratory analysis. In addition, another four HR-Peeper probes were deployed as above in a subsequent study to measure dissolved Mn(II) and Mn(III).

2.3. Porewater and solid-phase analyses

All metal(loid) analyses were performed under trace-metal clean conditions using acid-cleaned plasticware. The porewater samples were diluted (30−50 times) with acidified Milli-Q water for metal(loid) analysis to avoid the impacts of high salt concentrations (Wang and Wang, 2016). The metal(loid) concentrations in the acidified samples were determined by inductively coupled plasma mass spectrometry (ICP-MS, Agilent 7700X) with an internal standard (Agilent P/N 5183-4682) to correct for the instrument drift and physical interferences. The dissolved P concentration in the porewater was determined by miniaturized spectrophotometry methods using an Epoch microplate spectrophotometer (Bio Tek, Winooski, VT). Sulfate was determined using ion chromatography (Dionex, ICS 1600, USA). Dissolved Mn(II) and Mn(III) complexes were simultaneously determined using the porphyrin method developed by Madison et al. (2011).

The ZrO-AgI binding gels were cut along the open window and scanned by a flat-bed scanner (Canon 5600F). The scanned images were then converted into grayscale intensities with ImageJ. The accumulated mass (M_S, $\mu g\,cm^{-2}$) of the DGT-labile S was calculated using the calibration curve of the grayscale density (y) versus M_S (x) (Ding et al., 2012):

$$y = -171e^{-x/7.23} + 220 \tag{1}$$

Then, M_S was converted into the flux of the DGT-labile S (F_{DGT}, pg $cm^{-2}\,s^{-1}$) by dividing by the deployment time.

The solid samples were immediately freeze-dried at $-80\,°C$, and the dried samples were ground and sieved for further analysis. Afterwards, the labile P and Fe were extracted using an ascorbic acid solution in a single-step procedure to extract the reactive solid-phase P pool bound to amorphous iron (ASC-P), as well as amorphous iron (ASC-Fe) (Rozan et al., 2002). The P and Fe concentrations in the extracting solution were also determined by miniaturized spectrophotometry methods. The total nitrogen (TN) and total organic carbon (TOC) concentrations were determined using a Vario EL III element analyzer (Elementar, Germany). The particle size was measured using a Mastersizer 2000 (Malvern Instruments Ltd., UK.). A modified European Community Bureau of Reference (BCR) sequential extraction (three-step) procedure was employed to extract the Co, Cr, V, As and Mn fractions (Rauret et al., 1999). The extractants used for the three extractions were acetic acid (F1), hydroxylamine hydrochloride (F2) and hydrogen peroxide/ammonium acetate (F3), corresponding to the three fractions of exchangeable/carbonate, reducible and oxidizable matter, respectively. The metal(loid) concentrations in the extracting solutions were also determined by ICP-MS.

Method blanks, standard materials, and duplicates were used to guarantee quality control and quality assurance. Quality control samples were repeatedly measured after every 10 to 20 samples. Three replicates were used for the determination of the metal(loid) and P concentrations in the standard materials and samples, except porewater P due to the limited samples and TOC contents in the sediments. The average values of recovery of the standard materials and relative standard deviation (RSD) values of the samples are shown in Table S1.

2.4. Calculation of the benthic flux

The concentrations of the dissolved metal(loid)s and P in the vicinity of the SWI (1 cm above and below) at the submerged sites (JRE-5 and JRE-6) were used to calculate the benthic diffusion fluxes of metal(loid)s and P across the SWI. The diffusion flux (F) was calculated based on Fick's first law according to Eq. (2) (Ding et al., 2015), and the degree of sediment tortuosity (θ) was calculated using Eq. (3) (Boudreau, 1996):

$$F = F_w + F_p = -D_w\left(\frac{\delta c}{\delta x_w}\right)_{(x=0)} - \frac{\varphi D_p}{\theta^2}\left(\frac{\delta c}{\delta x_p}\right)_{(x=0)} \tag{2}$$

$$\theta^2 = 1 - \ln\left(\varphi^2\right) \tag{3}$$

where F_w and F_p are the flux from the overlying water to the porewater and the flux from the porewater to the overlying water, respectively; $(\delta c/\delta x_p)_{(x=0)}$ and $(\delta c/\delta x_w)_{(x=0)}$ are the concentration gradients of the dissolved metal(loid)s and P in the porewater and overlying water, respectively; φ is the porosity of the sediments; D_p and D_w are the diffusion coefficients of the metal(loid)s and P in the sediments and overlying water, respectively; and D_p was calculated from D_w via multiplying by φ^2 for $\varphi \geq 0.7$ (Li and Gregory, 1974; Ullman and Aller, 1982).

3. Results and discussion

3.1. Overlying water and sediment properties

The overlying water properties during low-tide time are shown in Table S2, and Table S3 shows the dissolved Fe, Mn, Co, Cr, V, Se, As and P concentrations in the overlying water compared to the defined standards. The concentrations of dissolved Co, Cr, V and As did not exceed the threshold values of the National Surface Water Environmental Quality Standards (GB3838-2002) grade I or standard values nor the Sea Water Quality Standard (GB 3097-1997) grade I in China. However, the dissolved Mn, Se and P concentrations exceeded different grades of the threshold values of both standards (Table S3). These results indicated potential water pollution with excessive amounts of Mn, Se and P in the JRE.

The particle size results indicated that the primary sediment type was clayey silt (Fig. S1). As shown in Fig. 2, the TOC contents, ranging from 1.02% to 1.57% among the six sediment cores, basically exhibited maxima in the subsurface layer and decreased with depth. The average values showed no notable differences between the six sites. The ASC-Fe and ASC-P contents also showed little difference between the six sites, although the contents exhibited fluctuations with varying degrees in each core. The ASC-Fe and ASC-P contents had consistent variations with significant positive correlations in all profiles, confirming that P sequestration is dominated by amorphous Fe (hydr)oxides (Rozan et al., 2002).

The distributions of the average values of the Mn, Co, Cr, V and As fractions in the sediment cores are shown in Fig. 3, and the whole fraction distributions with depth in the six sediment cores are shown in Figs. S2–S6. It is generally accepted that metal(loid) fractions in the F1, F2 and F3 forms have the potential to be mobilized from sediments and thus could become bioavailable (Yin et al., 2014; Gao et al., 2017). Compared with the intertidal sites (JRE-1 to JRE-4), the submerged sites (JRE-5 and JRE-6) had higher contents of the mobile fractions (sum of F1, F2 and F3), except for Co, which exhibited little difference among the six sites, possibly due to the intense reductive dissolution of F2 fractions at the submerged sites and because Co sulfide is more soluble than other metal sulfides (Saito et al., 2003). In particular, the Mn and As at the submerged sites had higher F1, lower F2 and more stable F3 levels than those at the intertidal sites. These differences reflected the transformation of some of the reducible fraction into exchangeable or/and carbonate fractions; the Co at the submerged sites had slightly higher F3, lower F2 and more stable F1 levels than those at the intertidal sites, reflecting the transformation of some of the reducible fraction into the oxidizable fraction; the Cr and V at the submerged sites had higher F1 and F3 and more stable (or lower in terms of the percentage) F2 levels than those at the intertidal sites, reflecting the transformation of some of the reducible fraction to exchangeable/carbonate and oxidizable fractions. All these variations indicate that a stronger geochemical cycling of metal(loid)s occurs at the submerged sites.

As shown in Fig. 2, DGT-Labile S fluxes were generally low in uppermost several centimeters then rapidly increased to relatively high levels and fluctuated to the bottom. Except for JRE-2, the average fluxes increased and the depth of the minimal flux deepened from JRE-1 to JRE-6 consecutively, which can be attributed to the bioturbation and radial oxygen loss by plant roots suppressing sulfate reduction at JRE-1 and JRE-3 and long-lasting flooding by overlying water fueling anoxic sulfate reduction at JRE-5 and JRE-6. Sulfate concentrations decreased with depth to different degrees, and the consumption was basically consistent with the increase in DGT-Labile S at the six sites, which could be regarded as an important indicator for sulfate reduction and sulfide accumulation. Nevertheless, the DGT-Labile S fluxes in this study were quite low (generally lower than $20 \, \text{pg cm}^{-2} \, \text{s}^{-1}$), which were even lower than those in lake sediments (Ding et al., 2012), indicating quite feeble sulfate reduction.

3.2. Mn and Fe redox cycling

Figs. 4 and 5 show the depth profiles and box plots, respectively, of the dissolved Fe, Mn, Co, Cr, V, Se, As and P concentrations in the porewater. The average values of these profiles are shown in Table S4. The dissolved Fe and Mn concentrations were the lowest or undetectable in the uppermost layers, then gently or suddenly increased at certain depths, followed by fluctuating and slightly declining to the bottom for the Mn concentration and mostly suddenly decreasing to the bottom for the Fe concentration. Compared with those in Mn, the fluctuations in Fe were drastic in both the subsurface layers and bottom layers. The average values at these sites showed no notable differences at the intertidal sites, excluding the three highest points at JRE-4, while the Mn concentrations at the submerged sites (nearly or exceeding $10 \, \text{mg L}^{-1}$) were significantly higher than those of Fe (less than $2 \, \text{mg L}^{-1}$) and much higher than those of Mn at the intertidal sites (mostly less than $2 \, \text{mg L}^{-1}$).

As oxygen and nitrate are depleted with depth, the Mn(III/IV) and Fe(III) (oxyhydr)oxides act as major terminal electron acceptors for the oxidation of OC with the production of soluble Mn(II/III) and Fe(II) (Shaw et al., 1990). Fe(III) is a less energetically favorable terminal electron acceptor than Mn(III/IV) thermodynamically, so the pronounced elevation of dissolved Fe is usually posterior to the dissolved Mn (Fig. 4). However, Mn oxides are strong oxidants that can oxidize Fe(II) back into Fe(III) oxides, especially in shallow sediments when reactive Mn oxides have not yet been depleted. Hence, the drastic fluctuation in the dissolved Fe pattern is likely attributed to reoxidation by the abundant Mn oxides in the surface layers (Fig. S2) or coprecipitation with sulfide in the subsurface layers (Fig. 2). In addition, the OC oxidation-coupled Mn reduction will lead to the production of secondary manganese carbonate minerals such as rhodochrosite ($MnCO_3$) (Johnson et al., 2013). When intense Fe reduction occurs in the presence of Mn(III/IV) oxides, the produced Fe(II) will be reoxidized by the Mn(III/IV) oxides, leading to coprecipitation of reduced Mn(II) with carbonate. This phenomenon may explain the high carbonate Mn (F1, Fig. 3) content accompanied by relatively limited dissolved Mn and intervallic dissolved Fe (Fig. 4) levels at JRE-2 and JRE-3.

The dissolved Mn at the submerged sites exhibited a rapid increase immediately below the SWI together with significantly higher concentrations throughout the profiles, demonstrating that hypoxic conditions facilitate Mn reduction and production of dissolved Mn. However, the remarkable dissolved Mn concentrations (nearly $15 \, \text{mg L}^{-1}$) were also higher than those in other studies on both marine sediment (less than $11 \, \text{mg L}^{-1}$, (Madison et al., 2013)) and lake sediments (several mg L^{-1}, (Fan et al., 2019)), suggesting intense Mn reduction in this region. Moreover, the intense Mn reduction appears to restrain Fe reduction as the dissolved Fe concentrations were moderate, especially in the context of hypoxia and sufficient ASC-Fe relative to the intertidal sites (Fig. 2). Therefore, Mn reduction is the dominant geochemical process for OC degradation and directly affects Fe cycling by the competitive inhibition of Fe(III) reduction and Fe(II) reoxidation. As a result, the reactive ASC-Fe presented no clear consumption or even somewhat increased with depth at all sites (Fig. 2).

Dissolved Mn(III), likely stabilized by organic or inorganic ligands, is primarily formed by oxidation of Mn(II) diffusing from anoxic porewater (Madison et al., 2011). As shown in Fig. S7, dissolved Mn(III) was also detected mainly in surface layers in this study, which was in agreement with the pattern observed in a
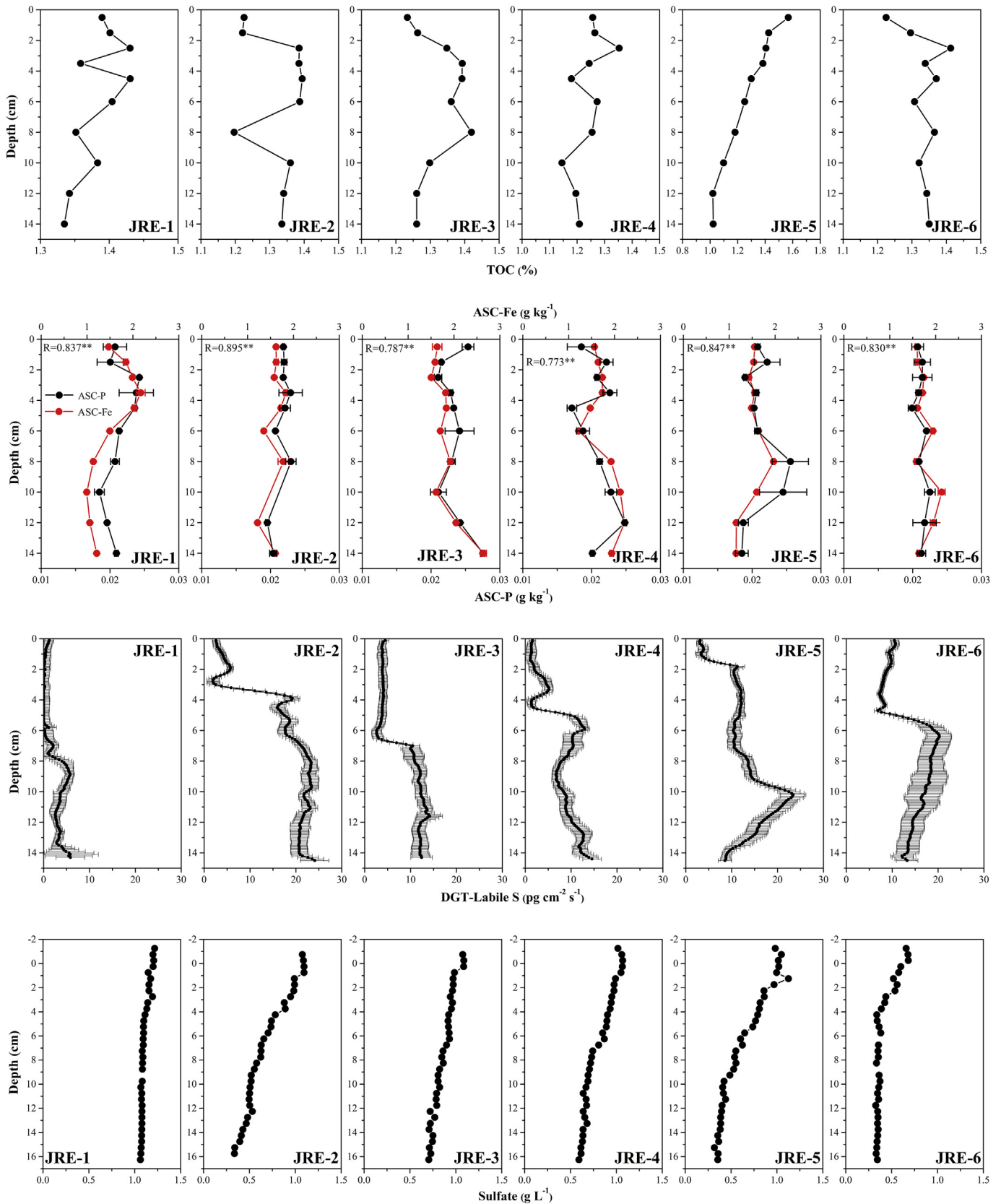
Fig. 2. Vertical distributions of the sediment TOC contents, ASC-P contents, ASC-Fe contents, DGT-Labile S fluxes and porewater sulfate concentrations. The correlations between the ASC-P and ASC-Fe contents are shown in the figure with ** denoting significance at the p < 0.01 level.
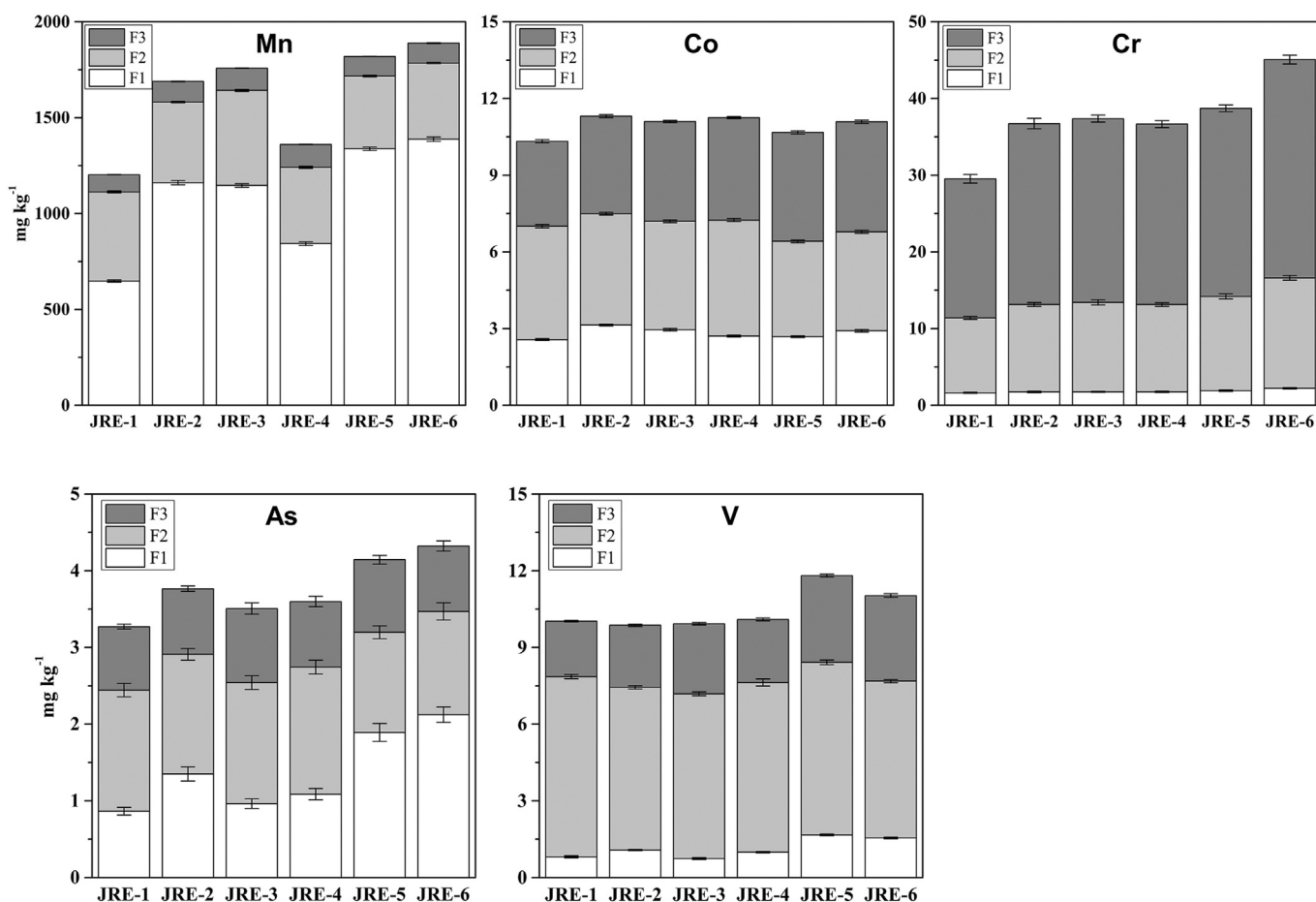
Fig. 3. Distributions of the average values of the Mn, Co, Cr, V and As fractions in the sediment cores.

previous study (Madison et al., 2013). Dissolved Mn(III) complexes can potentially serve as both reductants with oxygen and oxidants with sulfide or other low-valent metal(loid)s in one-electron-transfer reactions (Madison et al., 2013). The suboxic redox conditions measured in the previous study were also favored the existence of dissolved Mn(III) (Pan et al., 2019). Considering its ubiquity in surface porewaters, dissolved Mn(III) could facilitate key electron-transfer processes in biogeochemical cycles.

3.3. Changes in the dissolved metal(loid)s and P and their mobilization

As traditional redox-sensitive elements, the average vertical heterogeneity indexes (reflected by the RSDs of the vertically dissolved concentrations) (Chen et al., 2019a) among the six profiles of the dissolved Mn, Fe, P and As were 69%, 152%, 39% and 63%, respectively, while that of Co was 63%. All of these values were much greater than those of Cr (10%), V (14%) and Se (16%). The dissolved Cr, V and Se concentrations were quite stable in the vertical direction in most profiles, except several apparent high-value points and areas. In addition, Cr, V and Se were somewhat enriched in the surface porewater layer, which was opposite to the distributions of redox-sensitive elements such as Mn and Fe. In contrast, similar to Mn and Fe, the dissolved Co, As and P concentrations in most profiles were low in the uppermost layers, then gently or suddenly increased with depth, followed by a stabilization stage or a slight decline to the bottom. Among these elements, however, Co exhibited several apparent high-value points and areas

at JRE-4, JRE-5 and JRE-6; P presented very notable fluctuations throughout the entire profile at JRE-1, JRE-2 and JRE-3 with relatively low P concentrations.

3.3.1. Cr, V and Se

The lack of observed decrease or increase trends in the dissolved Cr, V and Se distributions in the vertical direction were similar to previous studies (Gao et al., 2017; Fan et al., 2019) together with low vertical heterogeneity indexes, demonstrating that the mobility levels of Cr, V and Se were not sensitive to changes in the redox conditions to a certain degree. In addition, the significant positive correlations among the dissolved Cr, V and Se (Table 1) and analogous distributions of the Cr and V fractions in the sediments (Fig. 3) indicate a homologous origin and fate of these elements, which may be cocaptured and coreleased in sediments and porewater during the same geochemical processes.

Dissolved Cr, V and Se show significant positive correlations with Mn and no correlations with Fe (Table 1 and Fig. S8), suggesting that the mobility levels of Cr, V and Se are more associated with Mn cycling but not with Fe cycling in this study. Fe (hydr) oxides are generally believed to be the dominant factor controlling metal(loid) mobility levels due to their ubiquitous presence in the supergene environment (Shaw et al., 1990; Bose and Sharma, 2002). However, Mn oxides have been found to supersede Fe(III) oxides in trapping metal(loid)s in recent years, and their mobility is mainly controlled by the absorption and reductive dissolution of Mn oxides (Beck et al., 2010; Fan et al., 2019). Moreover, different extents of hypoxia have been revealed to facilitate the
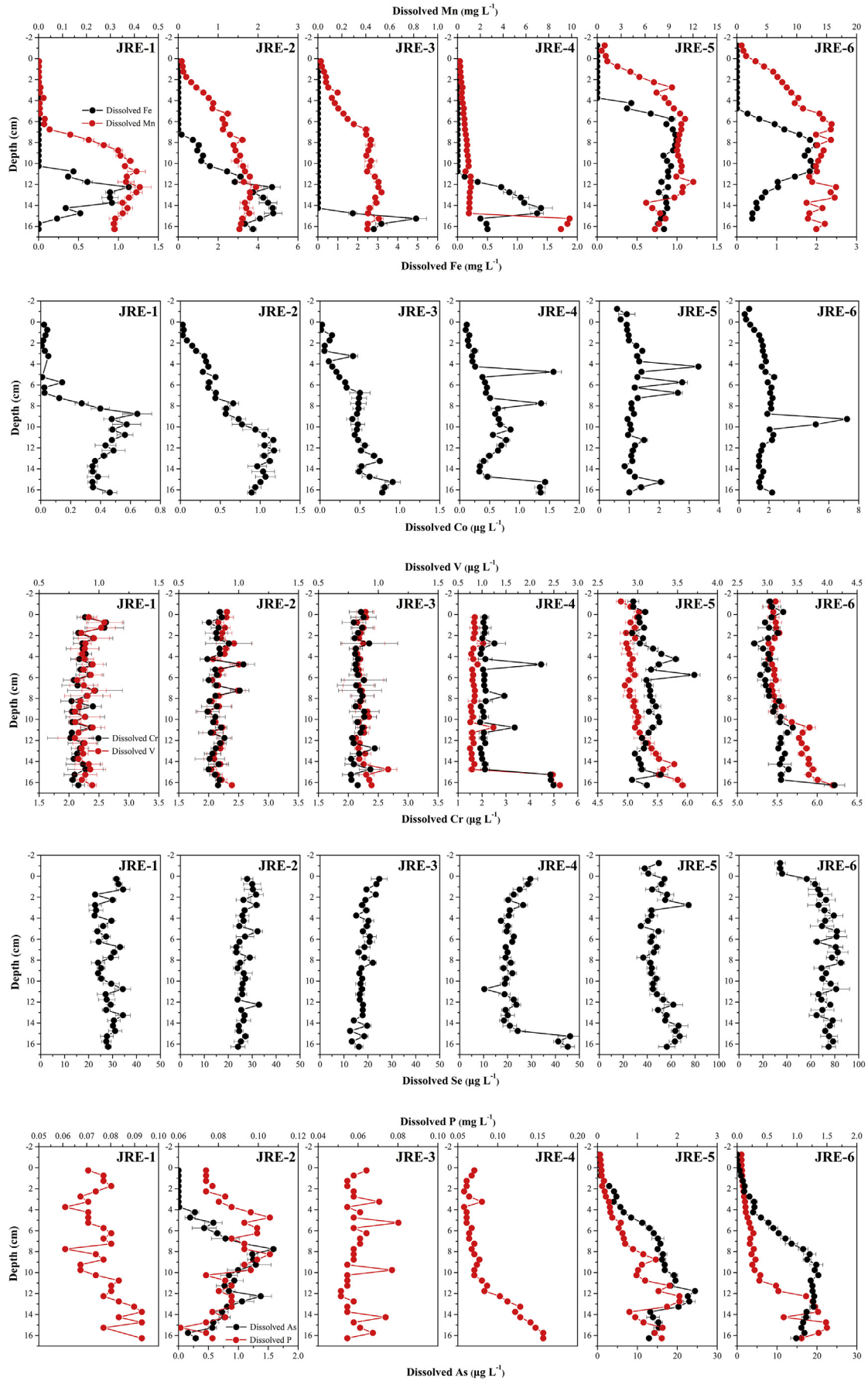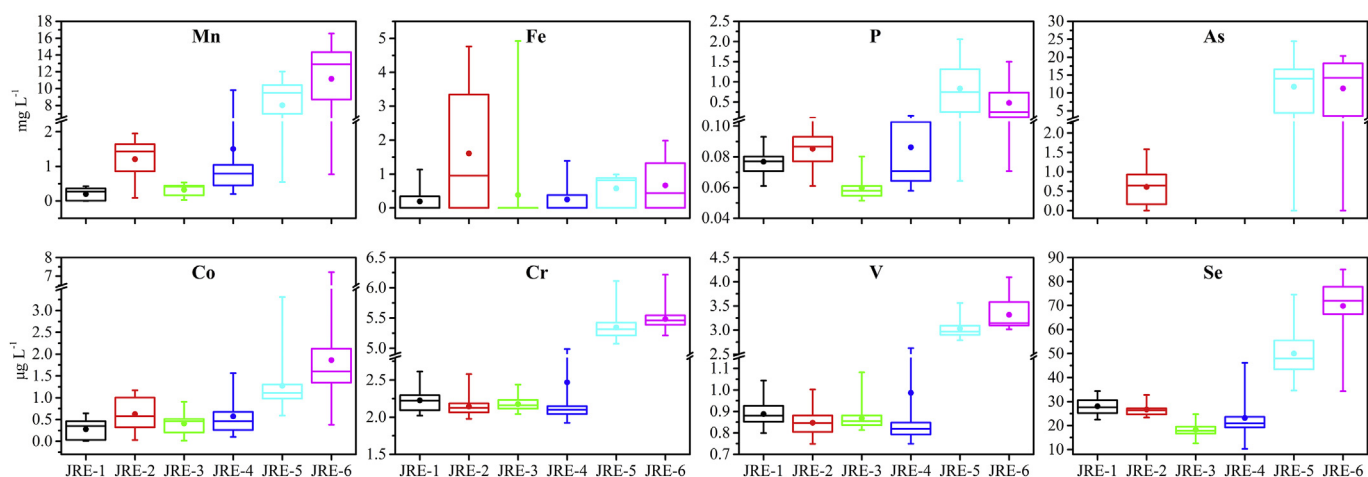
Fig. 4. Depth profiles of the dissolved Fe, Mn, Co, Cr, V, Se, As and P concentrations in the porewater of the six sampling sites.

Fig. 5. Box plot of the porewater Fe, Mn, Co, Cr, V, Se, As (μg L^{-1}) and P levels at the six sampling sites. The error bars represent the minimum and maximum in each profile.

biogeochemical cycling and liberation of heavy metals into the overlying water (Banks et al., 2012; Jin et al., 2019; Liu et al., 2019). In this study, we believe that the elevated dissolved Cr, V and Se concentrations at the submerged sites are attributed to the strengthened Mn reduction (which mineralizes OM) induced by hypoxia, as the positive correlations between metal(loid)s and Mn are even better than previously reported (Jin et al., 2019; Fan et al., 2019).

The moderate enrichment of the dissolved Cr, V and Se in the surface oxic layer may be explained by the existence of Mn(III) complexes in surface porewater (Fig. S7), as these complexes can oxidize the inert low-valent metal(loid)s into mobile high-valent metal(loid)s such as Cr(III) to Cr(VI) (Madison et al., 2013). In addition, the observation that the dissolved Cr, V and Se covaried very notably but not exactly with the dissolved Mn in all profiles (Fig. 4) suggests differences in their sources or rates and degrees of mobilization with Mn reduction (Beck et al., 2010). This phenomenon may reflect the relative dominance of Mn oxide adsorption versus metal(loid) coprecipitation (e.g., the partial coprecipitation with sulfide at JRE-2 with intense sulfate reduction), as well as stabilization by dissolved ligands (e.g., OM). These factors may explain the apparent high-value points for the different metal(loid) s at the different depths. However, the other apparent high-value areas of Cr, V, Se and Co at the bottom profile of JRE-4 should be attributed to the reductive dissolution of Mn oxides coupled with degradation of heterogeneous labile OM under suitable pH and redox conditions (Stockdale et al., 2009).

3.3.2. Co

The peak-pattern distribution pattern and high vertical heterogeneity index (63%) of the dissolved Co were similar to those of the redox-sensitive elements, such as Mn and Fe, which has been encountered earlier in both field and laboratory studies (Wang et al., 2016; Chen et al., 2017). The adsorption of Co(II) and Co(III) to the surface sites on Fe(III) (oxyhydr)oxides (Musić et al., 1979) and Mn(III, IV) oxides (Takahashi et al., 2007), respectively, are important pathways for the immobilization of Co under oxic conditions. Dissolved Co maxima may occur in conjunction with both dissolved Fe and Mn peaks (Viollier et al., 1995), indicating that Co can be released from the reductive dissolution of both Fe(III) (oxyhydr)oxides and Mn(III, IV) oxides (Swanner et al., 2014). In this study, Co was the only element exhibiting positive correlations with both Fe and Mn (Table 1 and Fig. S8). However, Co(III) is reduced to Co(II) in a similar Eh-pH space in which Mn(IV)

reduction occurs (Takahashi et al., 2007), while iron reduction occurs under more anoxic conditions than Co and Mn at marine pH values (~8, Table S2). Previous work has also found that Co mobility is mainly controlled by the absorption and reductive dissolution of Mn oxides, with r > 0.9 between DGT-Labile Co and Mn (Wang et al., 2016). This finding may be the reason that the dissolved Co had a more positive correlation with Mn than with Fe. In addition, Co was the only element remaining tightly coupled with Mn in all six profiles (r > 0.85), possibly because Co sulfide is more soluble than the sulfides of some other metals, such as Fe (Saito et al., 2003). In view of the relative weak sulfate reduction and DGT-labile S fluxes (Fig. 2), most sulfide should coprecipitate with dissolved Fe(II) or Fe(III) oxides.

3.3.3. As and P

P retention is generally regarded as being associated with Fe(III) (oxyhydr)oxides, while P remobilization could be associated with both the reductive dissolution of Fe(III)-bound P and the diagenetic decomposition of reactive organic P (Rozan et al., 2002; Kraal et al., 2015; Ding et al., 2018b). In light of the weak Fe(III) reduction and the lack of a clear consumption or even somewhat increased ASC-P level with depth (Fig. 2), the diagenetic decomposition of reactive organic P during intense microbial Mn reduction should be the dominant process for P remobilization and liberation into the porewater at the submerged sites. However, at the intertidal sites, the prevailing reoxidation of Fe(II) to Fe(III) by Mn(III/IV) oxides recovered the capacity of P sequestration, together with a relatively weak Mn reduction and drastically varying Fe reduction, thereby sustaining a low degree of P remobilization and complicating the dissolved P distributions with very notable fluctuations throughout the profiles. As a result, the positive correlation of P with Mn was weaker than those of the other metal(loid)s with Mn (Table 1), demonstrating the Fe-dependent and Mn-independent adsorption/ release of P (Chen et al., 2019b).

The significant positive correlation between As and Mn also verifies that the mobility of As is closely associated with the redox cycling of Mn oxides. The oxidation and adsorption at manganite surfaces has been revealed under oxic conditions to exhibit low dissolved As concentrations (Chiu and Hering, 2000), while As can be remobilized and released into porewater from the reductive dissolution of Mn oxides and/or reduction of the adsorbed As(V) to As(III) under anoxic conditions with weaker affinity levels with minerals (Bose and Sharma, 2002). Moreover, the As in sediments may also be remobilized due to the competitive desorption by

Table 1
Linear correlations between the porewater Fe, Mn, Co, Cr, V, Se, As and P levels.

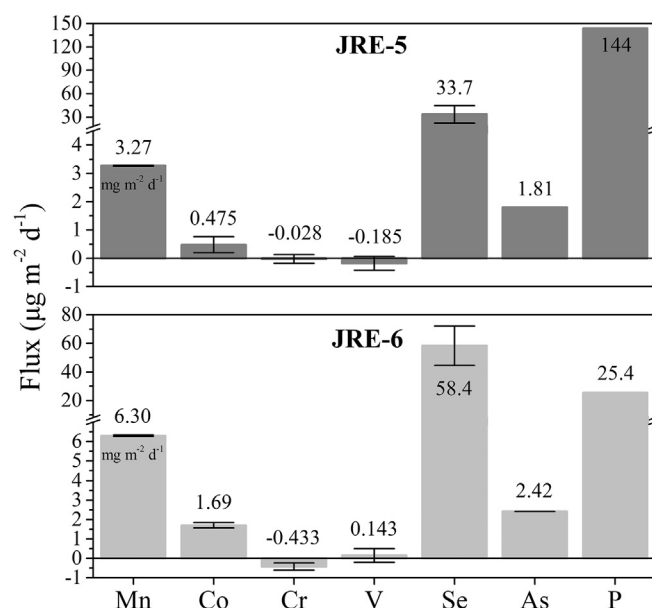|	Fe	Mn	Co	Cr	V	Se	As	P
Fe	1							
Mn	0.155	1						
Co	0.296*	0.744**	1					
Cr	−0.009	0.866**	0.665**	1				
V	0.008	0.881**	0.644**	0.984**	1			
Se	0.056	0.881**	0.670**	0.866**	0.901**	1		
As	0.004	0.857**	0.496**	0.657**	0.695**	0.616**	1	
P	0.075	0.662**	0.319*	0.614**	0.662**	0.538**	0.808**	1

$^*p < 0.05$; $^{**}p < 0.01$.

competing oxyanions, especially P, which has been considered a basic mechanism leading to the release of As (Smedley and Kinniburgh, 2002). Phosphate shares similar physiochemical properties with As (arsenate in particular), both of which occupy similar adsorption sites on iron/manganese oxides (Sun et al., 2017). Previous studies have verified that elevated P concentrations ($0.2 \, mg \, L^{-1}$) can obviously compete with As for the surface sites in sediments and correspondingly increase the liberation of As (Jiao et al., 2012; Sun et al., 2017), thereby leading to covaried patterns of the dissolved As and P, as also been found in this study (Fig. 4 and Table 1). In addition, analogous mechanisms have been revealed for V, Mo and Se (Brinza et al., 2008; Gao et al., 2017). The sequestrated metal(loid)s can be remobilized by anion exchange, particularly at the high concentrations of P at the submerged sites (greater than $2 \, mg \, L^{-1}$), which may be another reason in addition to Mn redox cycling for the positive correlations between all the metal(loid)s and P (Table 1).

It is evident that most of the metal(loid) and P distributions in this study are controlled by the redox cycling of the geochemical carrier Mn but not by that of Fe. Mn played a particularly significant role, presumably due to the greater sorptive capacities of its solid oxide surfaces for transition metal cations (Beck et al., 2010). The pH values measured in the previous study in this region ranged from 8.2 to 8.9 and decreased with depth (Pan et al., 2019). Alkaline conditions are also believed to be beneficial for metal adsorption by Fe/Mn hydroxides (Jia et al., 2007). In these coastal shallow sediments, the abundant Mn oxides and the tide-induced periodic redox migration may be responsible for the tight coupling of the metal(loid)s with Mn but not with Fe. When Fe(III) (oxyhydr)oxides are reduced, most of the dissolved Fe(II) will be removed from the porewater by reoxidation or sulfide precipitation. At shallow depths, Fe(II) is in excess relative to sulfide, and FeS is more soluble than other trace metal sulfides (Morel and Hering, 1993). Therefore, a greater proportion of Fe(II) than the other metals is recycled back into the oxyhydroxide phase. Over the course of tidal oscillations, Fe may undergo multiple reduction-oxidation cycles, and each time the newly formed Fe(III) (oxyhydr)oxides will have fewer scavenged trace metals (Kalnejais et al., 2015). However, the released metal(loid)s from Fe(III) reduction may still be retained by the abundant Mn oxides, leading to a higher proportions of Mn oxide-bound metal(loid)s; these metal(loid)s can be remobilized due to the intense reductive dissolution of Mn oxides, presenting tightly coupled patterns between the dissolved Mn and metal(loid)s.

3.4. Diffusion fluxes of Mn, Co, Cr, V, Se, As and P across the SWI

The concentration gradients of the dissolved Mn, Co, Cr, V, Se, As and P were visible from the profiles in both the porewater and overlying water layers in the vicinity of the SWI at the submerged sites (Fig. 4). The calculation results of the diffusion fluxes are shown in Fig. 6. The considerable diffusion fluxes of Mn are on the

Fig. 6. Diffusion fluxes of Mn, Co, Cr, V, Se, As and P across the SWI at JRE-5 and JRE-6.

same order of magnitude as those reported in the research on mangrove coasts in Australia, which are greater than the estimated fluxes from riverine and atmospheric sources (Holloway et al., 2016), demonstrating that the mangrove ecosystem may be a major player in the oceanic cycle of Mn. The diffusion fluxes of the other redox-sensitive elements such as Co, As and P were also positive, indicating that porewater acts as a source of Co, As and P that can be transported into the overlying water, which is closely coupled with the Mn cycle. For the remaining redox-insensitive elements, the diffusion fluxes of Cr and V are low and partially negative, while the positive diffusion fluxes of Se are much higher than those of any other metal(loid)s and even comparable to that of P, implying a severe Se pollution source from the porewater.

The trapping and recycling of metal(loid)s by Mn oxides result in metal(loid) remobilization in reducing sediments and partial enrichment in the surface porewater (Shaw et al., 1990). This process is particularly favored by the oscillating redox cycling induced by the tide to stimulate the Mn cycle in this coastal environment, leading to continuous metal(loid) liberation into the overlying water. It is worth noting that the high diffusion fluxes of Mn, P and Se are in line with the high levels of Mn, P and Se in the overlying water, which exceed the defined standards (Table S3), demonstrating that sediment Mn reduction and concomitant metal(loid) and P remobilization can be vital pathways for metal(loid) and P migration to the overlying water, which may pose potential hazards to estuarine and coastal ecosystems.

4. Conclusions

As the visualized reflections of early diagenetic reactions and geochemical cycling in sediments, the contaminant characteristics in porewater are also vital in relating sediments and the overlying water. Based on high-resolution dialysis and DGT technology, the dissolved Fe, Mn, Co, Cr, V, Se, As and P concentrations in porewater and DGT-Labile S in sediment can be used to determine the kinetic mechanism that drives the remobilization of metal(loid)s and P in coastal sediments and their benthic exchange fluxes. The distributions of the mobile fractions of metal(loid)s in the sediment cores reveal that a stronger geochemical cycling of metal(loid)s occurs at the submerged sites. Mn(III/IV) reduction dominates the

diagenetic pathway for OC degradation and directly affects Fe cycling by the competitive inhibition of Fe(III) reduction at the hypoxic submerged sites and Fe(II) reoxidation at the aerobic intertidal sites.

The significant positive correlations between the dissolved Co, Cr, V, Se, As and P with Mn and nearly no correlations between these elements with Fe demonstrate that the mobility levels of these metal(loid)s and P are more associated with Mn cycling but not with Fe cycling; these elements are scavenged by Mn(III/IV) oxides under oxic conditions and remobilized due to the reductive dissolution of Mn(III/IV) oxides coupled with OM degradation under hypoxic/anoxic conditions. The sufficient solid Mn oxides, greater sorptive capacities of its solid oxide surfaces for transition metal cations, and tide-induced periodic redox migration are responsible for the tight coupling of metal(loid)s with Mn. In addition, hypoxia facilitates the liberation of metal(loid)s and P via enhanced Mn reduction. However, the mobility of Cr, V and Se is somewhat insensitive to changes in the redox conditions, and these elements may have homologous origins and fates. The diagenetic decomposition of organic P by Mn reduction should be a major pathway for P remobilization. The high diffusion fluxes of Mn, P and Se through the SWI and the high levels of Mn, P and Se in the overlying water could be harmful to estuarine and coastal ecosystems.

Acknowledgments

Appendix A. Supplementary data

Supplementary data to this article can be found online at https://doi.org/10.1016/j.envpol.2019.113134.

References

Banks, J.L., Ross, D.J., Keough, M.J., Eyre, B.D., Macleod, C.K., 2012. Measuring hypoxia induced metal release from highly contaminated estuarine sediments during a 40 day laboratory incubation experiment. Sci. Total Environ. 420, 229–237. https://doi.org/10.1016/j.scitotenv.2012.01.033.

Beck, A.J., Cochran, J.K., Sanudo-Wilhelmy, S.A., 2010. The distribution and speciation of dissolved trace metals in a shallow subterranean estuary. Mar. Chem. 121, 145–156. https://doi.org/10.1016/j.marchem.2010.04.003.

Bose, P., Sharma, A., 2002. Role of iron in controlling speciation and mobilization of arsenic in subsurface environment. Water Res. 36, 4916–4926. https://doi.org/10.1016/s0043-1354(02)00203-8.

Boudreau, B.P., 1996. The diffusive tortuosity of fine-grained unlithified sediments. Geochem. Cosmochim. Acta 60, 3139–3142. https://doi.org/10.1016/0016-7037(96)00158-5.

Brinza, L., Benning, L.G., Satham, P.J., 2008. Adsorption studies of Mo and V onto ferrihydrite. Mineral. Mag. 72, 385–388. https://doi.org/10.1180/minmag.2008.072.1.385.

Chen, M., Ding, S., Gao, S., Fu, Z., Tang, W., Wu, Y., Gong, M., Wang, D., Wang, Y., 2019a. Efficacy of dredging engineering as a means to remove heavy metals from lake sediments. Sci. Total Environ. 665, 181–190. https://doi.org/10.1016/j.scitotenv.2019.02.057.

Chen, M., Ding, S., Wu, Y., Fan, X., Jin, Z., Tsang, D.C.W., Wang, Y., Zhang, C., 2019b. Phosphorus mobilization in lake sediments: experimental evidence of strong control by iron and negligible influences of manganese redox reactions. Environ. Pollut. 246, 472–481. https://doi.org/10.1016/j.envpol.2018.12.031.

Chen, M., Ding, S., Zhang, L., Li, Y., Sun, Q., Zhang, C., 2017. An investigation of the effects of elevated phosphorus in water on the release of heavy metals in sediments at a high resolution. Sci. Total Environ. 575, 330–337. https://doi.org/10.1016/j.scitotenv.2016.10.063.

Chiu, V.Q., Hering, J.G., 2000. Arsenic adsorption and oxidation at manganite surfaces. 1. Method for simultaneous determination of adsorbed and dissolved arsenic species. Environ. Sci. Technol. 34, 2029–2034. https://doi.org/10.1021/es990788p.

Conley, D.J., Paerl, H.W., Howarth, R.W., Boesch, D.F., Seitzinger, S.P., Havens, K.E., Lancelot, C., Likens, G.E., 2009. ECOLOGY controlling eutrophication: nitrogen and phosphorus. Science 323, 1014–1015. https://doi.org/10.1126/science.1167755.

Davison, W., Zhang, H., 1994. In-situ speciation measurements of trace components in natural-waters using thin-film gels. Nature 367, 546–548.

Ding, S., Chen, M., Gong, M., Fan, X., Qin, B., Xu, H., Gao, S., Jin, Z., Tsang, D.C.W., Zhang, C., 2018a. Internal phosphorus loading from sediments causes seasonal nitrogen limitation for harmful algal blooms. Sci. Total Environ. 625, 872–884. https://doi.org/10.1016/j.scitotenv.2017.12.348.

Ding, S., Han, C., Wang, Y., Yao, L., Wang, Y., Xu, D., Sun, Q., Williams, P.N., Zhang, C., 2015. In situ, high-resolution imaging of labile phosphorus in sediments of a large eutrophic lake. Water Res. 74, 100–109. https://doi.org/10.1016/j.watres.2015.02.008.

Ding, S., Sun, Q., Chen, X., Liu, Q., Wang, D., Lin, J., Zhang, C., Tsang, D.C.W., 2018b. Synergistic adsorption of phosphorus by iron in lanthanum modified bentonite (Phoslock (R)): new insight into sediment phosphorus immobilization. Water Res. 134, 32–43. https://doi.org/10.1016/j.watres.2018.01.055.

Ding, S., Sun, Q., Xu, D., Jia, F., He, X., Zhang, C., 2012. High-resolution simultaneous measurements of dissolved reactive phosphorus and dissolved sulfide: the first observation of their simultaneous release in sediments. Environ. Sci. Technol. 46 (15), 8297–8304. https://doi.org/10.1021/es301134h.

Ellis, A.S., Johnson, T.M., Bullen, T.D., 2002. Chromium isotopes and the fate of hexavalent chromium in the environment. Science 295, 2060–2062. https://doi.org/10.1126/science.1068368.

Fan, X., Ding, S., Chen, M., Gao, S., Fu, Z., Gong, M., Tsang, D.C.W., Wang, Y., Zhang, C., 2019. Peak chromium pollution in summer and winter caused by high mobility of chromium in sediment of a eutrophic lake: in situ evidence from high spatiotemporal sampling. Environ. Sci. Technol. 53, 4755–4764. https://doi.org/10.1021/acs.est.8b07060.

Gao, B., Gao, L., Zhou, Y., Xu, D., Zhao, X., 2017. Evaluation of the dynamic mobilization of vanadium in tributary sediments of the Three Gorges Reservoir after water impoundment. J. Hydrol. 551, 92–99. https://doi.org/10.1016/j.jhydrol.2017.05.034.

Hamilton, S.J., 2004. Review of selenium toxicity in the aquatic food chain. Sci. Total Environ. 326, 1–31. https://doi.org/10.1016/j.scitotenv.2004.01.019.

Holloway, C.J., Santos, I.R., Tait, D.R., Sanders, C.J., Rose, A.L., Schnetger, B., Brumsack, H.-J., Macklin, P.A., Sippo, J.Z., Maher, D.T., 2016. Manganese and iron release from mangrove porewaters: a significant component of oceanic budgets? Mar. Chem. 184, 43–52. https://doi.org/10.1016/j.marchem.2016.05.013.

Jia, Y., Xu, L., Wang, X., Demopoulos, G.P., 2007. Infrared spectroscopic and X-ray diffraction characterization of the nature of adsorbed arsenate on ferrihydrite. Geochem. Cosmochim. Acta 71, 1643–1654. https://doi.org/10.1016/j.gca.2006.12.021.

Jiao, W., Chen, W., Chang, A.C., Page, A.L., 2012. Environmental risks of trace elements associated with long-term phosphate fertilizers applications: a review. Environ. Pollut. 168, 44–53. https://doi.org/10.1016/j.envpol.2012.03.052.

Jin, Z., Ding, S., Sun, Q., Gao, S., Fu, Z., Gong, M., Lin, J., Wang, D., Wang, Y., 2019. High resolution spatiotemporal sampling as a tool for comprehensive assessment of zinc mobility and pollution in sediments of a eutrophic lake. Journal of Hazardous Materials 364, 182–191. https://doi.org/10.1016/j.jhazmat.2018.09.067.

Johnson, J.E., Webb, S.M., Thomas, K., Ono, S., Kirschvink, J.L., Fischer, W.W., 2013. Manganese-oxidizing photosynthesis before the rise of cyanobacteria. Proc. Natl. Acad. Sci. U. S. A 110, 11238–11243. https://doi.org/10.1073/pnas.1305530110.

Kalnejais, L.H., Martin, W.R., Bothner, M.H., 2015. Porewater dynamics of silver, lead and copper in coastal sediments and implications for benthic metal fluxes. Sci. Total Environ. 517, 178–194. https://doi.org/10.1016/j.scitotenv.2015.02.011.

Kankanmge, N.R., Bennett, W.W., Teasdale, P.R., Huang, J., Welsh, D.T., 2017. Comparing in situ colorimetric DET and DGT techniques with ex situ core slicing and centrifugation for measuring ferrous iron and dissolved sulfide in coastal sediment pore waters. Chemosphere 188, 119–129. https://doi.org/10.1016/j.chemosphere.2017.08.144.

Khademi, H., Abbaspour, A., Martinez-Martinez, S., Gabarron, M., Shahrokh, V., Faz, A., Acosta, J.A., 2018. Provenance and environmental risk of windblown materials from mine tailing ponds, Murcia, Spain. Environ. Pollut. 241, 432–440. https://doi.org/10.1016/j.envpol.2018.05.084.

Kraal, P., Burton, E.D., Rose, A.L., Kocar, B.D., Lockhart, R.S., Grice, K., Bush, R.T., Tan, E., Webb, S.M., 2015. Sedimentary iron-phosphorus cycling under contrasting redox conditions in a eutrophic estuary. Chem. Geol. 392, 19–31. https://doi.org/10.1016/j.chemgeo.2014.11.006.

Leermakers, M., Gao, Y., Gabelle, C., Lojen, S., Ouddane, B., Wartel, M., Baeyens, W., 2005. Determination of high resolution pore water profiles of trace metals in sediments of the Rupel River (Belgium) using DET (diffusive equilibrium in thin films) and DGT (diffusive gradients in thin films) techniques. Water Air Soil Pollut. 166, 265–286. https://doi.org/10.1007/s11270-005-6671-7.

Lin, P., Guo, L., Chen, M., Cai, Y., 2013. Distribution, partitioning and mixing behavior of phosphorus species in the Jiulong River estuary. Mar. Chem. 157, 93–105. https://doi.org/10.1016/j.marchem.2013.09.002.

Liu, J.-J., Diao, Z.-H., Xu, X.-R., Xie, Q., 2019. Effects of dissolved oxygen, salinity, nitrogen and phosphorus on the release of heavy metals from coastal sediments. Sci. Total Environ. 666, 894–901. https://doi.org/10.1016/j.scitotenv.2019.02.288.

Li, Y.-H., Gregory, S., 1974. Diffusion of ions in seawater and deep sea sediments.

Geochem. Cosmochim. Acta 38, 703–714.

Madison, A.S., Tebo, B.M., Luther III, G.W., 2011. Simultaneous determination of soluble manganese(III), manganese(II) and total manganese in natural (pore) waters. Talanta 84, 374–381. https://doi.org/10.1016/j.talanta.2011.01.025.

Madison, A.S., Tebo, B.M., Mucci, A., Sundby, B., Luther III, G.W., 2013. Abundant porewater Mn(III) is a major component of the sedimentary redox system. Science 341, 875–878. https://doi.org/10.1126/science.1241396.

Morel, F., Hering, J., 1993. Principles and Applications of Aquatic Chemistry. John Wiley and Sons, Inc., New York.

Musić, S., Gessner, M., Wolf, R.H.H., 1979. Sorption of small amounts of cobalt (II) on iron (III) oxide. Microchim. Acta 71 (1–2), 105–112.

Muyzer, G., Stams, A.J.M., 2008. The ecology and biotechnology of sulphate-reducing bacteria. Nat. Rev. Microbiol. 6 (6), 441–454. https://doi.org/10.1038/nrmicro1892.

Ni, Z., Zhang, L., Yu, S., Jiang, Z., Zhang, J., Wu, Y., Zhao, C., Liu, S., Zhou, C., Huang, X., 2017. The porewater nutrient and heavy metal characteristics in sediment cores and their benthic fluxes in Daya Bay, South China. Mar. Pollut. Bull. 124, 547–554. https://doi.org/10.1016/j.marpolbul.2017.07.069.

Pan, F., Liu, H., Guo, Z., Li, Z., Wang, B., Cai, Y., Gao, A., 2019. Effects of tide and season changes on the iron-sulfur-phosphorus biogeochemistry in sediment porewater of a mangrove coast. J. Hydrol. 568, 686–702. https://doi.org/10.1016/j.jhydrol.2018.11.002.

Pan, F., Liu, H., Guo, Z., Li, Z., Wang, B., Gao, A., 2017. Geochemical behavior of phosphorus and iron in porewater in a mangrove tidal flat and associated phosphorus input into the ocean. Cont. Shelf Res. 150, 65–75. https://doi.org/10.1016/j.csr.2017.09.012.

Rauret, G., Lopez-Sanchez, J.F., Sahuquillo, A., Rubio, R., Davidson, C., Ure, A., Quevauviller, P., 1999. Improvement of the BCR three step sequential extraction procedure prior to the certification of new sediment and soil reference materials. J. Environ. Monit. 1, 57–61. https://doi.org/10.1039/a807854h.

Rozan, T.F., Taillefert, M., Trouwborst, R.E., Glazer, B.T., Ma, S.F., Herszage, J., Valdes, L.M., Price, K.S., Luther, G.W., 2002. Iron-sulfur-phosphorus cycling in the sediments of a shallow coastal bay: implications for sediment nutrient release and benthic macroalgal blooms. Limnol. Oceanogr. 47, 1346–1354. https://doi.org/10.4319/lo.2002.47.5.1346.

Saito, M.A., Sigman, D.M., Morel, F.M.M., 2003. The bioinorganic chemistry of the ancient ocean: the co-evolution of cyanobacterial metal requirements and biogeochemical cycles at the Archean-Proterozoic boundary? Inorg. Chim. Acta 356, 308–318. https://doi.org/10.1016/s0020-1693(03)00442-0.

Sharma, V.K., Sohn, M., 2009. Aquatic arsenic: toxicity, speciation, transformations, and remediation. Environ. Int. 35, 743–759. https://doi.org/10.1016/j.envint.2009.01.005.

Shaw, T.J., Gieskes, J.M., Jahnke, R.A., 1990. Early diagenesis in differing depositional-environments — the response of transition-metals in pore water. Geochem. Cosmochim. Acta 54, 1233–1246. https://doi.org/10.1016/0016-7037(90)90149-f.

Smedley, P.L., Kinniburgh, D.G., 2002. A review of the source, behaviour and distribution of arsenic in natural waters. Appl. Geochem. 17, 517–568. https://doi.org/10.1016/s0883-2927(02)00018-5.

Stockdale, A., Davison, W., Zhang, H., 2009. Micro-scale biogeochemical heterogeneity in sediments: a review of available technology and observed evidence.

Earth Sci. Rev. 92, 81–97. https://doi.org/10.1016/j.earscirev.2008.11.003.

Sun, Q., Ding, S., Zhang, L., Chen, M., Zhang, C., 2017. A millimeter-scale observation of the competitive effect of phosphate on promotion of arsenic mobilization in sediments. Chemosphere 180, 285–294. https://doi.org/10.1016/j.chemosphere.2017.04.010.

Sundby, B., 2006. Transient state diagenesis in continental margin muds. Mar. Chem. 102, 2–12. https://doi.org/10.1016/j.marchem.2005.09.016.

Swanner, E.D., Planavsky, N.J., Lalonde, S.V., Robbins, L.J., Bekker, A., Rouxel, O.J., Saito, M.A., Kappler, A., Mojzsis, S.J., Konhauser, K.O., 2014. Cobalt and marine redox evolution. Earth Planet. Sci. Lett. 390, 253–263. https://doi.org/10.1016/j.epsl.2014.01.001.

Takahashi, Y., Manceau, A., Geoffroy, N., Marcus, M.A., Usui, A., 2007. Chemical and structural control of the partitioning of Co, Ce, and Pb in marine ferromanganese oxides. Geochem. Cosmochim. Acta 71, 984–1008. https://doi.org/10.1016/j.gca.2006.11.016.

Teasdale, P.R., Batley, G.E., Apte, S.C., Webster, I.T., 1995. Pore water sampling with sediment peepers. Trac. Trends Anal. Chem. 14, 250–256. https://doi.org/10.1016/0165-9936(95)91617-2.

Ullman, W.J., Aller, R.C., 1982. Diffusion coefficient in nearshore marine sediments. Limnol. Oceanogr. 27, 552–556. https://doi.org/10.4319/lo.1982.27.3.0552.

Viollier, E., Jézéquel, D., Michard, G., Pèpe, M., Sarazin, G., Alberic, P.J.C.G., 1995. Geochernical study of a crater lake (Pavin Lake, France): trace-element behaviour in the monimolimnion, 125, 61–72.

Wang, D., Gong, M., Li, Y., Xu, L., Wang, Y., Jing, R., Ding, S., Zhang, C., 2016. In situ, high-resolution profiles of labile metals in sediments of lake Taihu. Int. J. Environ. Res. Public Health 13. https://doi.org/10.3390/ijerph13090884.

Wang, W., Wang, W.-X., 2016. Phase partitioning of trace metals in a contaminated estuary influenced by industrial effluent discharge. Environ. Pollut. 214, 35–44. https://doi.org/10.1016/j.envpol.2016.03.059.

Wang, W., Wang, W.-X., 2017. Trace metal behavior in sediments of Jiulong River Estuary and implication for benthic exchange fluxes. Environ. Pollut. 225, 598–609. https://doi.org/10.1016/j.envpol.2017.03.028.

Wu, G., Cao, W., Huang, Z., Kao, C.-M., Chang, C.-T., Chiang, P.-C., Wang, F., 2017. Decadal changes in nutrient fluxes and environmental effects in the Jiulong River Estuary. Mar. Pollut. Bull. 124, 871–877. https://doi.org/10.1016/j.marpolbul.2017.09.002.

Xu, D., Wu, W., Ding, S., Sun, Q., Zhang, C., 2012. A high-resolution dialysis technique for rapid determination of dissolved reactive phosphate and ferrous iron in pore water of sediments. Sci. Total Environ. 421, 245–252. https://doi.org/10.1016/j.scitotenv.2012.01.062.

Yang, C., Li, Y., Zhou, Y., Zheng, W., Tian, Y., Zheng, T., 2012. Bacterial community dynamics during a bloom caused by Akashiwo sanguinea in the Xiamen sea area, China. Harmful Algae 20, 132–141. https://doi.org/10.1016/j.hal.2012.09.002.

Yin, H., Cai, Y., Duan, H., Gao, J., Fan, C., 2014. Use of DGT and conventional methods to predict sediment metal bioavailability to a field inhabitant freshwater snail (Bellamya aeruginosa) from Chinese eutrophic lakes. J. Hazard Mater. 264, 184–194. https://doi.org/10.1016/j.jhazmat.2013.11.030.

Zhang, H., Davison, W., Mortimer, R.J.G., Krom, M.D., Hayes, P.J., Davies, I.M., 2002. Localised remobilization of metals in a marine sediment. Sci. Total Environ. 296, 175–187. https://doi.org/10.1016/s0048-9697(02)00078-5.